Chemical Science

ROYAL SOCIETY OF CHEMISTRY

EDGE ARTICLE

View Article Online
View Journal | View Issue

Cite this: *Chem. Sci.*, 2024, **15**, 2946

All publication charges for this article have been paid for by the Royal Society of Chemistry

One-pot asymmetric living copolymerization-induced chiral self-assemblies and circularly polarized luminescence†

Run-Tan Gao,[a] Shi-Yi Li,[a] Bing-Hao Liu,[a] Zheng Chen,[a] Na Liu,*[b] Li Zhou[c] and Zong-Quan Wu*[a]

Received 22nd November 2023
Accepted 12th December 2023

DOI: 10.1039/d3sc06242b

rsc.li/chemical-science

Controlled synthesis of conjugated block polymers enables the optimization of their self-assembly and may lead to distinct optical properties and functionalities. Herein, we report a direct chain extension of one-handed helical poly(acyl methane) with 1-ethynyl-4-iodo-2,5-bis(octyloxy)benzene, affording well-defined π-conjugated poly(acyl methane)-*b*-poly(phenylene ethynylene) copolymers. Although the distinct monomers are polymerized *via* different mechanisms, the one-pot copolymerization follows a living polymerization manner, giving the desired optically active block copolymers with controllable molar mass and low distribution. The block copolymerization induced chiral self-assembly simultaneously due to the one-handed helicity of the poly(acyl methane) block, giving spherical nanoparticles, one-handed helices, and chiral micelles with controlled dimensions regarding the composition of the generated copolymers. Interestingly, the chiral assemblies exhibit clear circularly polarized luminescence with tunable handedness and a high dissymmetric factor.

Introduction

Chirality is ubiquitous in nature and plays important roles. For example, the basic structural units of biomacromolecules, such as amino acids and sugars, are all homochiral. Biopolymers also exhibit chirality in the form of one-handed helices, such as the double helix of DNA and the single right-handed helix of polypeptides and polysaccharides.[1–4] These chiral helices formed by biomacromolecules have indispensable functions, including stereospecific enzyme catalysis, genetic storage, replication and transcription.[5–7] Inspired by biological helices, significant efforts have been made to create synthetic helical polymers and supramolecular helical assemblies to develop optically active materials for applications in chirality resolution, asymmetric catalysis, and circularly polarized luminescence (CPL).[8–17] Fully organic CPL materials are particularly interesting because they emit CPL light directly and have potential applications in optical quantum information, data storage, and chirality sensing.[18–24]

Among the handful of methods that have been developed for the synthesis of helical materials, asymmetric polymerization of achiral monomers using a chiral catalyst/initiator is an effective strategy because it can produce large quantities of optically active helical polymers from achiral materials.[25,26] Notably, helical poly(acyl methane) (PAM) is a carbon–carbon main chain polymer that carries substituents on every backbone atom, and thus, can twist into stable helices in both a solid film and in solution.[27–34] Therefore, we recently developed chiral Pd(II)-catalysts bearing bidentate phosphine ligands that initiate an asymmetric living polymerization of achiral diazoacetates to give one-handed PAMs with predictable molar masses (M_n) and low dispersities (M_w/M_n).[35–38] We envisioned that the terminal Pd(II)-complex on the synthesized helical PAMs could be subsequently activated to initiate a block copolymerization of aryl monomers and fabricate π-conjugated block copolymers. The helical PAM block would then drive chiral self-assembly of the generated block copolymers during the polymerization, resulting in polymerization-induced self-assembly (PISA).[39–41] Thus, various well-defined supramolecular self-assembled architectures could be readily achieved. Moreover, the helical PAM block could also induce asymmetric self-assembly, and helical chirality transfer to the achiral π-conjugated block would give supramolecular architectures with chiroptical properties.

Conjugated polymers have generated considerable interest due to their promising potential in light-emitting materials and devices, and other similar fields.[42–45] To optimize the performance, fabricating π-conjugated block polymers with

[a]*State Key Laboratory of Supramolecular Structure and Materials, College of Chemistry, Jilin University, Changchun 130012, China. E-mail: zqwu@jlu.edu.cn*

[b]*The School of Pharmaceutical Sciences, Jilin University, 1266 Fujin Road, Changchun, Jilin 130021, P.R. China. E-mail: liuna606@jlu.edu.cn*

[c]*Department of Polymer Science and Engineering, Hefei University of Technology, Hefei 230009, China*

† Electronic supplementary information (ESI) available. See DOI: https://doi.org/10.1039/d3sc06242b

controlled morphologies is highly desired.[46–48] Conventional methods for synthesizing π-conjugated block copolymers include: (1) connection of the chain ends of two pre-formed homopolymers, and (2) functionalizing a homopolymer with an active chain end and then initiation of a copolymerization reaction with a second monomer.[49–52] However, these methods require tedious synthetic manipulation and are usually time-consuming. Therefore, developing new strategies for the facile synthesis of well-defined π-conjugated block polymers in a controllable fashion is highly desired. Among the reported π-conjugated polymers, poly(phenylene ethynylene)s (PPEs) have attracted growing interest over the past decade for their extensive use in light-emitting diodes, bacterial identification, explosives detection, and molecular wires.[53–55] Therefore, developing new strategies for the controlled synthesis of PPE block copolymers and controlling the resulting self-assembled morphology are important research aims.

Herein, we report the asymmetric coordination polymerization of achiral diazoacetate, naphthalen-2-ylmethyl 2-diazoacetate (**1**) using chiral Pd(II)-catalysts (*R*- and *S*–Pd(II)) to obtain one-handed helical PAMs (*R*- or *S*-poly-$\mathbf{1}_m$s) with chiral Pd(II)-complexes on the terminal chain end. Subsequent direct chain extension of the helical PAM polymers with 1-ethynyl-4-iodo-2,5-bis(octyloxy)benzene (**2**) in the same pot leads to optically active PAM-*b*-PPE copolymers (*R*- or *S*-poly($\mathbf{1}_m$-*b*-$\mathbf{2}_n$)). Although the polymerization mechanism and structure of the two monomers are different, the one-pot block copolymerization is a living polymerization reaction and yields PAM-*b*-PPE copolymers with predictable M_n and low M_w/M_n. Moreover, the chiral catalysts induce asymmetric polymerization, resulting in *R*- and *S*-poly-$\mathbf{1}_m$s with a preferred one-handed helix. The helical PAM block and intermolecular interactions of the added PPE block synergistically induce chiral self-assembly of the *in situ* generated *R*- or *S*-poly($\mathbf{1}_m$-*b*-$\mathbf{2}_n$) copolymers. Spherical micelles and one-handed helical nanofibers with high solid contents (*ca.* 53%) are facilely obtained. Remarkably, the chiral self-assemblies formed by the block copolymers exhibit interesting CPL with tunable handedness and a high dissymmetric factor.

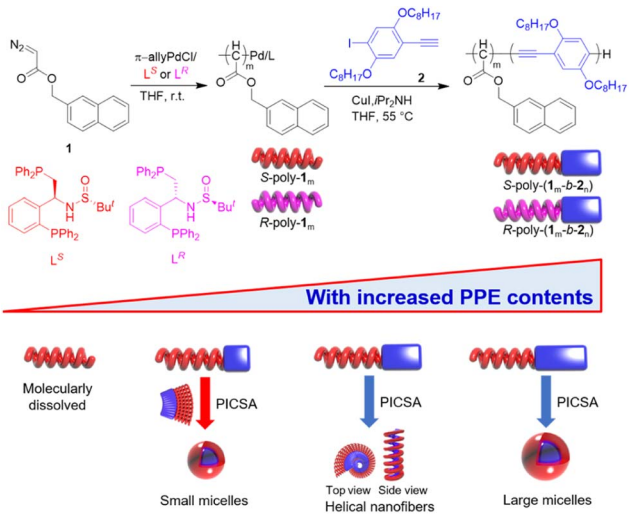

Scheme 1 Synthesis and self-assembly of poly($\mathbf{1}_m$-*b*-$\mathbf{2}_n$) copolymers.

Results and discussion

Hybrid block copolymerization

At room temperature, the one-pot block copolymerization was performed in tetrahydrofuran (THF). The chiral π-allyl Pd(II)-catalysts (*R*–Pd(II) or *S*–Pd(II)) with either *R*- or *S*-Wei-Phos were prepared following reported procedures.[32] As shown in Scheme 1, the *R*–Pd(II) catalyst was directly added to a THF solution containing monomer **1** ($[\mathbf{1}]_0/[Pd]_0 = 100$). Size exclusion chromatography (SEC) analysis (Fig. 1) showed that the resulting *R*-poly-$\mathbf{1}_m$ had an M_n of 4.7 kg mol^{-1} and M_w/M_n of 1.15 (run 1, Table 1). To this *R*-poly-$\mathbf{1}_m$ solution, a THF solution containing monomer **2**, cuprous iodide, and diisopropylamine was added directly ($[\mathbf{2}]_0/[Pd]_0 = 100$). After 12 h, the polymerization was quenched by precipitating the solids into *n*-hexane, and the polymer was isolated with a 90% yield over the two steps. The SEC trace of the resulting *R*-poly($\mathbf{1}_m$-*b*-$\mathbf{2}_n$) block copolymer showed a unimodal elution peak. The peak of the block copolymer appeared at a higher M_n compared to that of the *R*-poly-$\mathbf{1}_m$ precursor (Fig. 1a). As determined by SEC, the M_n increased to 12.1 kg mol^{-1} and the dispersity remained low with $M_w/M_n = 1.18$. The degrees of polymerization (DPs) of the two blocks deduced from ^{1}H NMR analyses are 105 and 98, which generally agree with the feed ratios of the two monomers; thus, the *R*-homopolymer and the block copolymer were denoted as *R*-poly-$\mathbf{1}_{105}$ and *R*-poly($\mathbf{1}_{105}$-*b*-$\mathbf{2}_{98}$), respectively (see below). High-M_n copolymers could also be prepared by this method. For instance, the copolymerization of **2** with *R*-poly-$\mathbf{1}_{105}$ yielded the expected *R*-poly($\mathbf{1}_{105}$-*b*-$\mathbf{2}_{250}$) with an M_n of 30.5 kg mol^{-1} and $M_w/M_n = 1.10$ (Fig. S1, ESI†).

To verify the living nature of the copolymerization reaction, a series of block copolymers were prepared using a common Pd(II)-terminated *R*-poly-$\mathbf{1}_{105}$ ($M_n = 4.7$ kg mol^{-1}, $M_w/M_n = 1.15$) block and varying **2**-to-Pd(II) ratios. The block copolymerization proceeded smoothly and resulted in the expected *R*-poly($\mathbf{1}_{105}$-*b*-$\mathbf{2}_n$) copolymers in high yields (runs 2–7, Table 1). SEC traces of these copolymers contained single peaks that moved to higher M_n values with increasing **2**-to-Pd(II) ratios (Fig. 1a), and the M_n values of the copolymers varied linearly with the **2**-to-Pd(II) ratio (Fig. 1b). Furthermore, all block copolymers had low dispersities with $M_w/M_n < 1.25$. These results confirm that the

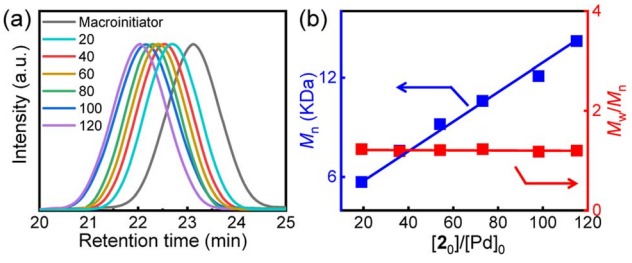

Fig. 1 (a) SEC curves for the copolymerization of **2** initiated by *R*-poly-$\mathbf{1}_{105}$ carrying the Pd(II)-terminus at different **2**-to-Pd(II) ratios. (b) Plots of M_n and M_w/M_n of *R*-poly($\mathbf{1}_m$-*b*-$\mathbf{2}_n$)s *vs.* the **2**-to-Pd(II) ratios.

Table 1 The results for the one-pot block copolymerization

Run	Polymer[a]	M_n[b] (kg mol^{-1})	M_w/M_n[b]	Yield[c]
1	*R*-Poly-$\mathbf{1}_{105}$	4.7	1.15	83%
2	*R*-Poly($\mathbf{1}_{105}$-*b*-$\mathbf{2}_{19}$)	5.7	1.23	75%
3	*R*-Poly($\mathbf{1}_{105}$-*b*-$\mathbf{2}_{36}$)	7.6	1.19	74%
4	*R*-Poly($\mathbf{1}_{105}$-*b*-$\mathbf{2}_{54}$)	9.2	1.21	76%
5	*R*-Poly($\mathbf{1}_{105}$-*b*-$\mathbf{2}_{73}$)	10.6	1.23	78%
6	*R*-Poly($\mathbf{1}_{105}$-*b*-$\mathbf{2}_{98}$)	12.1	1.18	74%
7	*R*-Poly($\mathbf{1}_{105}$-*b*-$\mathbf{2}_{115}$)	14.2	1.20	78%
8	*S*-Poly-$\mathbf{1}_{105}$	5.9	1.16	85%
9	*S*-Poly($\mathbf{1}_{105}$-*b*-$\mathbf{2}_{25}$)	6.2	1.16	78%
10	*S*-Poly($\mathbf{1}_{105}$-*b*-$\mathbf{2}_{52}$)	9.8	1.19	85%
11	*S*-Poly($\mathbf{1}_{105}$-*b*-$\mathbf{2}_{95}$)	11.9	1.21	79%
12	Poly-$\mathbf{2}_{30}$	6.9	1.19	90%

[a] The polymers were prepared according to Scheme 1 and the DPs were determined by ^{1}H NMR analyses. The polymers were named according to the feed ratios used in their synthesis. [b] The M_n and M_w/M_n were calculated by SEC. [c] Isolated yields in two steps.

block copolymerization proceeded *via* a living chain-growth reaction.

To gain further insights into the living nature of the block copolymerization reaction, Pd(II)-terminated *R*-poly-$\mathbf{1}_{105}$ (M_n = 4.7 kg mol^{-1}, M_w/M_n = 1.15) was used as a macroinitiator to polymerize **2** ([**2**]$_0$/[Pd]$_0$ = 100). The reaction progress was followed with SEC. As displayed in Fig. 2a, the peaks in the SEC traces gradually shifted to shorter times as the reaction progressed and remained unimodal and symmetrical throughout the entire polymerization. Likewise, the calculated M_n of the block copolymer increased linearly with the conversion of **2** (Fig. 2b) while M_w/M_n remained <1.25. It was found that >84% of **2** was consumed in 4 h, suggesting that the copolymerization was quite fast (Fig. 2c). The conversion of **2** followed first-order reaction kinetics, and the apparent polymerization rate constant was 1.63 × 10^{-4} s^{-1}. These results further confirmed that the one-pot block copolymerization of the two distinct monomers proceeded in a living polymerization fashion, albeit with different polymerization mechanisms and monomer structures. Utilizing this method, a series of PAM-*b*-PPE copolymers with expected M_n and low M_w/M_n values were prepared by varying the ratio of the catalyst to the two monomers (runs 2–7, Table 1). Similarly, the *S*-poly-$\mathbf{1}_m$ homopolymer and the corresponding *S*-poly($\mathbf{1}_m$-*b*-$\mathbf{2}_n$) copolymers were prepared using the *S*–Pd(II) catalyst (Scheme 1, and runs 8–11, Table 1). A poly-$\mathbf{2}_{30}$ homopolymer was also prepared as a control experiment (run 12, Table 1, see the ESI† for details).

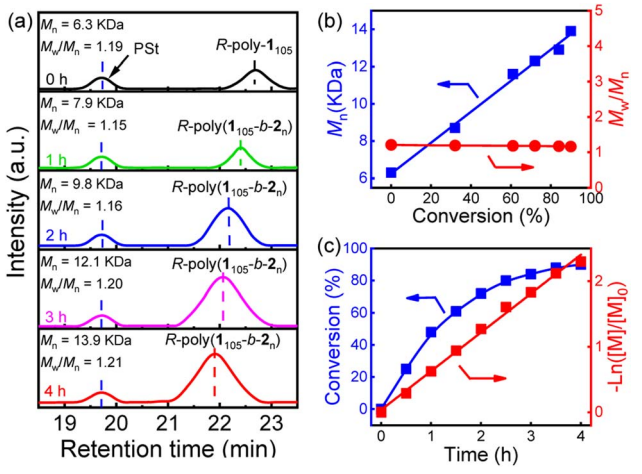

Fig. 2 (a) Time-dependent SEC for the copolymerization of **2** catalyzed by Pd(II)-terminated *R*-poly-$\mathbf{1}_{105}$. (b) Plots of M_n and M_w/M_n of *R*-poly($\mathbf{1}_m$-*b*-$\mathbf{2}_n$) *vs.* the conversion of **2**. (c) Plots of conversion and −ln([*M*]/[*M*]$_0$) values *vs.* the polymerization time.

^{1}H NMR spectra confirmed the chemical structure of the synthesized PAM-*b*-PEE copolymers (Fig. 3). For instance, the spectrum of *R*-poly($\mathbf{1}_{105}$-*b*-$\mathbf{2}_{98}$) showed characteristic resonance peaks corresponding to both the *R*-poly-$\mathbf{1}_{105}$ and poly-$\mathbf{2}_{98}$ blocks (Fig. 3a and b). The peaks corresponding to the ArH (*a*) and OCH_2 (*b*) in the poly-$\mathbf{2}_{98}$ segment appeared at 7.01 and 4.02 ppm, respectively, while the ArH (*c*) and $ArCH_2$ (*d*) resonances attributable to the *R*-poly-$\mathbf{1}_{105}$ block were located at 7.59–6.50 and 5.14–4.31 ppm, respectively. The peaks corresponding to the CH (*e*) groups in the poly-$\mathbf{1}_{105}$ backbone were between 4.22 and 3.34 ppm in the ^{1}H NMR spectrum of *R*-poly($\mathbf{1}_{105}$-*b*-$\mathbf{2}_{98}$). The integration of the $ArCH_2$ (5.14–4.31) from poly-$\mathbf{1}_m$ and OCH_2 (4.02) from poly-$\mathbf{2}_n$ gave a block ratio of nearly 105 : 98, which was in good agreement with the ratio of the monomers used in the block copolymerization owing to the living polymerization mechanism of the copolymerization and almost quantitative conversions of the monomers. The complementary FT-IR spectra of *R*-poly($\mathbf{1}_{105}$-*b*-$\mathbf{2}_{98}$) also showed vibrations corresponding to the *R*-poly-$\mathbf{1}_{105}$ and poly-$\mathbf{2}_{98}$ blocks (Fig. S2, ESI†). Thermogravimetric analysis (TGA) of *R*-poly($\mathbf{1}_{105}$-*b*-$\mathbf{2}_{98}$) showed two decomposition temperatures corresponding to the PAM and PPE blocks (Fig. S3, ESI†). In contrast, the differential scanning calorimetry (DSC) profile of *R*-poly($\mathbf{1}_{105}$-*b*-$\mathbf{2}_{98}$) showed glass transition (T_g, 60 °C) and melting (T_m, 220 °C) temperatures assignable to PPE (T_m = 220 °C) and PAM (T_g = 50 °C) segments (Fig. S4, ESI†). These studies confirmed the formation of the expected block copolymers.

Polymerization-induced chiral self-assembly

The chiral Pd(II)-catalysts induced the asymmetric polymerization of achiral monomer **1**. Thus, the CD spectra of *R*- and *S*-poly-$\mathbf{1}_{105}$ polymers showed clear positive and negative absorption peaks, respectively, due to the formation of one-handed helices (Fig. S5, ESI†). The optical activity of these polymers remained stable over a temperature range of −10 to 55 °C and in various solvents, regardless of their polarity; thus, suggesting the formation of highly stable helical structures in *R*- and *S*-poly-$\mathbf{1}_m$s. (Fig. S6 and S7, ESI†). The chiral Pd(II) catalysts selectively polymerized the achiral monomer **1**, forming block copolymers with chiral self-assembly. As seen in Fig. 4a, the solution of *R*-poly-$\mathbf{1}_{105}$ is nearly colorless. In contrast, the solutions of the *R*-poly($\mathbf{1}_{105}$-*b*-$\mathbf{2}_n$)s copolymers exhibited light green and yellow colors depending on the length of the poly-$\mathbf{2}_n$ block, which is attributed to the π-conjugated structure of the poly-$\mathbf{2}_n$ block. Furthermore, the absorption and circular dichroism (CD) spectra of *R*-poly-$\mathbf{1}_m$ and corresponding *R*-

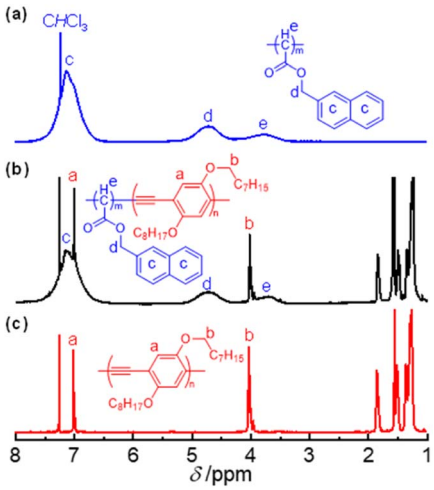

Fig. 3 ^{1}H NMR ($CDCl_3$, 600 MHz) spectra of the polymers: *R*-poly-$\mathbf{1}_{105}$ (a), *R*-poly($\mathbf{1}_{105}$-*b*-$\mathbf{2}_{98}$) (b), and poly-$\mathbf{2}_{30}$ (c) measured at room temperature.

poly($\mathbf{1}_m$-*b*-$\mathbf{2}_n$) copolymers were recorded and are shown in Fig. 4b. In *R*-poly-$\mathbf{1}_{105}$, the CD spectrum displayed absorption only between 205 and 325 nm, while the copolymer exhibited an additional intense absorption band between 325 and 510 nm. The molecular absorption between 325 and 510 nm increases as the length of the PPE block increases, and is accompanied by a red shift (Fig. 4b).

The CD spectra of the block copolymers showed absorption in the wavelength region of the achiral PPE segment, which was counterintuitive. For instance, the CD spectrum of *R*-poly($\mathbf{1}_{105}$-*b*-$\mathbf{2}_n$) had a positive signal between 330 and 510 nm, while that of *S*-poly($\mathbf{1}_m$-*b*-$\mathbf{2}_n$) showed a negative peak in the same wavelength region. The *R*-poly($\mathbf{1}_{105}$-*b*-$\mathbf{2}_{54}$) and *S*-poly($\mathbf{1}_{105}$-*b*-$\mathbf{2}_{52}$), with similar DPs, showed mirror-imaged CD spectra. The PPE (poly-$\mathbf{2}_n$) block is a linear π-conjugated system and does not contain chiral moieties. Thus, the CD signal at longer wavelengths was likely due to the chiral self-assembly of the generated block copolymers. The *g*(CD) ($\Delta\varepsilon/\varepsilon$) values at longer wavelengths increased with increasing PPE blocks and reached the maximum when the DP of PPE reached 73. With a further increase in the DP of PPE, the CD of the PPE block decreased. This can be attributed to the self-assembly of block copolymers with different PPE lengths into different supramolecular architectures. For instance, the *g*(CD) at 460 nm was +1.65 × 10^{-4} for *R*-poly($\mathbf{1}_{105}$-*b*-$\mathbf{2}_{19}$), +2.76 × 10^{-4} for *R*-poly($\mathbf{1}_{105}$-*b*-$\mathbf{2}_{36}$), +3.38 × 10^{-4} for *R*-poly($\mathbf{1}_{105}$-*b*-$\mathbf{2}_{54}$), and +4.12 × 10^{-4} for *R*-poly($\mathbf{1}_{105}$-*b*-$\mathbf{2}_{73}$), respectively. Furthermore, the *g*(CD) values decreased after the DP of PPE was higher than 73. For instance, the *g*(CD) at 460 nm was +3.42 × 10^{-4} for *R*-poly($\mathbf{1}_{105}$-*b*-$\mathbf{2}_{98}$) and 2.69 × 10^{-4} for *R*-poly($\mathbf{1}_{105}$-*b*-$\mathbf{2}_{115}$) (Fig. S8, ESI†). Intriguingly, temperature-dependent CD spectra measured *via* cooling–heating cycles indicated that the CD intensity between 250 and 300 nm came from the helicity of the poly-$\mathbf{1}_m$ block kept constant upon heating from 25 to 55 °C. The CD intensity of the aggregated poly-$\mathbf{2}_m$ segment (330–510 nm) gradually decreased upon heating, completely disappeared at 55 °C for 6 h, and could be restored after cooling the solution to room temperature (Fig. 4c). This result suggested that the macromolecular helicity of the poly-$\mathbf{1}_m$ block was thermally stable. In contrast, the block copolymers formed chiral self-assemblies at low temperatures that disassembled at high temperatures. The CD and absorption analyses indicated that the optical activity of the PPE block was due to the formation of chiral self-assembled structures. It is also worth noting that the signals in the CD spectra of the block copolymer between 205–245 and 250–320 nm from the *R*-poly-$\mathbf{1}_m$ block did not change significantly upon heating. This suggested that the PAM segment formed a highly stable helix even in the block copolymer. Thus, it was concluded that the chirality of the *R*–Pd(II)-catalyst was first transferred to the *R*-poly-$\mathbf{1}_m$ block *via* the asymmetric polymerization of the achiral monomer **1**, resulting in poly-$\mathbf{1}_m$ polymers with one-handed helicity. The helical chirality was transferred to the PPE block of the generated PAM-*b*-PPE copolymer *via* chiral self-assembly. Note that the chain extension of the structurally distinct PPE block induced a microphase separation of the resulting PAM-*b*-PPE copolymers and promoted the π–π stacking of the π-conjugated PPE segments. Owing to the chirality of helical PAM, the block copolymer asymmetrically self-assembles into various chiral supramolecular architectures depending on the helicity of PAM and the block ratio of the two blocks (Scheme 1). Through the asymmetric self-assembly, the PAM helical chirality was transferred to the supramolecular architectures, endowing the aggregated-PPE block with high optical activity and intense CD signals. Compared to the spherical aggregates, the compacted stacking of PPE blocks in helical nanofibers showed higher CD intensity.

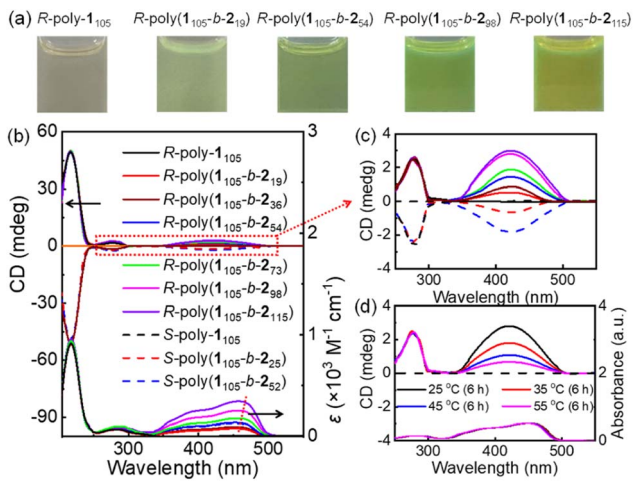

Fig. 4 (a) Photographs of *R*-poly($\mathbf{1}_{105}$-*b*-$\mathbf{2}_n$) copolymers under room light in THF. (b) CD and UV-vis absorption spectra of poly($\mathbf{1}_{105}$-*b*-$\mathbf{2}_n$) copolymers (THF, 25 °C). (c) Amplified CD spectra of poly($\mathbf{1}_{105}$-*b*-$\mathbf{2}_n$) copolymers (THF, 25 °C). (d) CD and UV-vis absorption spectra of poly($\mathbf{1}_{105}$-*b*-$\mathbf{2}_n$) copolymers measured in THF at different temperatures.

The polymerization-induced chirality transfer led us to investigate the morphology of the self-assembled structures. Atomic force microscopy (AFM) images of the structures formed by block copolymers isolated at different polymerization stages are shown in Fig. 5. It was found that *R*-poly($\mathbf{1}_{105}$-*b*-$\mathbf{2}_{19}$) with

a short PPE block formed spherical nanoparticles with the approximate diameter of *ca.* 48 nm. The spherical nanoparticles were likely core–shell micelles with a PPE core and helical PAM shell. *R*-poly($\mathbf{1}_{105}$-*b*-$\mathbf{2}_{36}$) with a slightly longer PPE block self-assembled into right-handed helical nanofibers (Fig. 5b), which agreed with the CD spectrum. Similarly, *R*-poly($\mathbf{1}_{105}$-*b*-$\mathbf{2}_{54}$) and *R*-poly($\mathbf{1}_{105}$-*b*-$\mathbf{2}_{73}$), with longer PPE blocks, also formed right-handed helical nanofibers (Fig. 5c and d), whereas *R*-poly($\mathbf{1}_{105}$-*b*-$\mathbf{2}_{98}$), with longer PPE blocks, formed broader nanofibers (Fig. 5e). Note that the diameter of the helical nanofibers increased with the DP of the PPE segment in the block copolymers. Specifically, the approximate diameters were 62, 82, 142, and 184 nm for *R*-poly($\mathbf{1}_{105}$-*b*-$\mathbf{2}_{36}$), *R*-poly($\mathbf{1}_{105}$-*b*-$\mathbf{2}_{54}$), *R*-poly($\mathbf{1}_{105}$-*b*-$\mathbf{2}_{73}$), and *R*-poly($\mathbf{1}_{105}$-*b*-$\mathbf{2}_{98}$), respectively. Meanwhile, *R*-poly($\mathbf{1}_{105}$-*b*-$\mathbf{2}_{115}$), with the longest PPE block, formed larger spherical aggregates with a diameter of approximately 200 nm (Fig. 5f). Since the self-assembly of PAM-*b*-PPE copolymers was mainly induced by the microphase separation of the structurally distinct blocks, the chain-length ratio of the two blocks plays an important role in the self-assembly morphology. The copolymers composed of the two blocks with a similar DP of each block tend to self-assemble into helical fibres. In comparison, the large differences in the DPs of the two blocks tend to self-assemble into spherical aggregates.

The morphologies of the polymerization-induced chiral assemblies were further confirmed by transmission electron microscopy (TEM). As shown in Fig. 6a, spherical micelles of ~52 nm diameter were seen in the TEM image of *R*-poly($\mathbf{1}_{105}$-*b*-$\mathbf{2}_{19}$). In contrast, the TEM images of *R*-poly($\mathbf{1}_{105}$-*b*-$\mathbf{2}_{54}$), *R*-poly($\mathbf{1}_{105}$-*b*-$\mathbf{2}_{73}$), and *R*-poly($\mathbf{1}_{105}$-*b*-$\mathbf{2}_{98}$) copolymers, with different PPE lengths, showed nanofibril morphologies (Fig. 6b–e). In agreement with the AFM results, TEM images showed that *R*-poly($\mathbf{1}_{105}$-*b*-$\mathbf{2}_{115}$) self-assembled into core–shell micelles of ~220 nm diameter (Fig. 6f). Overall, similar morphologies were seen in both the TEM and AFM images.

To verify that the helicity of the self-assembled nanofibers originated from the chiral Pd(II)-catalyst, the morphologies of the structures formed by the block copolymers prepared using the *S*–Pd(II)-catalyst were also investigated by AFM. As seen in Fig. S9 and S10 in ESI,† *S*-poly($\mathbf{1}_{105}$-*b*-$\mathbf{2}_{25}$) and *S*-poly($\mathbf{1}_{105}$-*b*-$\mathbf{2}_{155}$) self-assembled into spherical aggregates with approximate diameters of 45 and 205 nm, respectively, and formed very similar structures to those seen in *R*-poly($\mathbf{1}_{105}$-*b*-$\mathbf{2}_{19}$) and *R*-poly($\mathbf{1}_{105}$-*b*-$\mathbf{2}_{115}$). As anticipated, *S*-poly($\mathbf{1}_{105}$-*b*-$\mathbf{2}_{32}$), *S*-poly($\mathbf{1}_{105}$-*b*-$\mathbf{2}_{52}$), and *S*-poly($\mathbf{1}_{105}$-*b*-$\mathbf{2}_{95}$) formed nanofibril morphologies. However, these fibres were twisted into left-handed helices, *i.e.*, the opposite helicity to those prepared using the *R*–Pd(II) catalyst. These results agreed well with the CD analyses and further confirmed that the helicity of the polymerization-induced chiral assemblies was determined by the chirality of the Pd(II)-catalysts. Interestingly, the mixture of *R*- and *S*-copolymers showed different self-assembly morphologies to those of the *R*- and *S*-copolymers. For instance, the equivalent mixtures of *R*-poly($\mathbf{1}_{105}$-*b*-$\mathbf{2}_{54}$) and *S*-poly($\mathbf{1}_{105}$-*b*-$\mathbf{2}_{52}$) self-assembled into spherical nanoparticles under the same conditions described above (Fig. S11–S12, ESI†), probably due to the intermolecular interaction between the *R*- and *S*-copolymers. Detailed studies revealed that the solid content in the polymerization-induced self-assemblies was up to 53% (Fig. S13, ESI†).

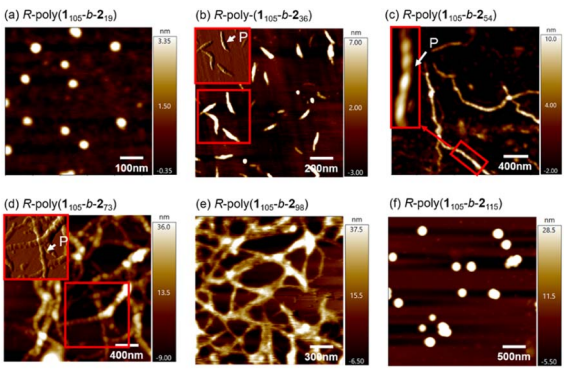

Fig. 5 AFM images of *R*-poly($\mathbf{1}_{105}$-*b*-$\mathbf{2}_{19}$) (a), *R*-poly($\mathbf{1}_{100}$-*b*-$\mathbf{2}_{36}$) (b), *R*-poly($\mathbf{1}_{105}$-*b*-$\mathbf{2}_{54}$) (c), *R*-poly($\mathbf{1}_{105}$-*b*-$\mathbf{2}_{73}$) (d), and *R*-poly($\mathbf{1}_{105}$-*b*-$\mathbf{2}_{98}$) (e), and *R*-poly($\mathbf{1}_{105}$-*b*-$\mathbf{2}_{115}$) (f).

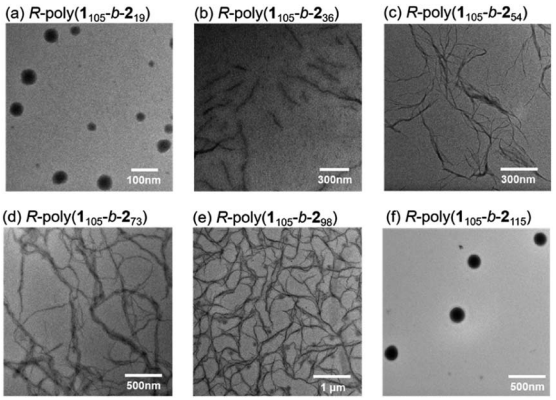

Fig. 6 TEM images of *R*-poly($\mathbf{1}_{105}$-*b*-$\mathbf{2}_{19}$) (a), *R*-poly($\mathbf{1}_{105}$-*b*-$\mathbf{2}_{36}$) (b), *R*-poly($\mathbf{1}_{105}$-*b*-$\mathbf{2}_{54}$) (c), *R*-poly($\mathbf{1}_{105}$-*b*-$\mathbf{2}_{73}$) (d), and *R*-poly($\mathbf{1}_{105}$-*b*-$\mathbf{2}_{98}$) (e), and *R*-poly($\mathbf{1}_{105}$-*b*-$\mathbf{2}_{115}$) (f).

CPL properties

It is well known that PPE is a good photoluminescent material; thus, the emission of PAM-*b*-PPE copolymers was also investigated. As displayed in Fig. 7, *R*-poly-$\mathbf{1}_m$ showed no emission, while the *R*-poly($\mathbf{1}_{105}$-*b*-$\mathbf{2}_m$) copolymers showed a strong blue emission at 475 and 505 nm. The emission intensities increased as the length of the PPE segment increased, accompanied by a slight red shift (Fig. 7b). As seen in the emission spectra, the poly($\mathbf{1}_{105}$-*b*-$\mathbf{2}_n$) copolymers emitted light between 450 and 550 nm with a maximum emission at 475 nm (Fig. 7b). Interestingly, the chiral self-assemblies of the block copolymers showed clear CPL. As summarized in Fig. 7c, *R*-poly($\mathbf{1}_{105}$-*b*-$\mathbf{2}_m$) exhibited positive CPL between 420 and 600 nm when irradiated at 380 nm. At the same time, the *S*-poly($\mathbf{1}_{105}$-*b*-$\mathbf{2}_{52}$) showed negative CPL in the same wavelength region under the same irradiation conditions. Interestingly, the dissymmetric factor ($|g_{\mathrm{lum}}|$) also depended on the DP of PPE, similar to that of g(CD). It first increased with the increase in the DP of PPE and reached

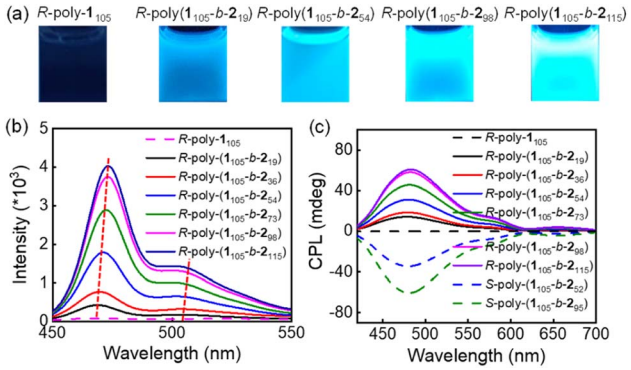

Fig. 7 (a) Photographs of poly($\mathbf{1}_{105}$-*b*-$\mathbf{2}_n$) copolymers under UV light of 365 nm. (b) Emission spectra of poly($\mathbf{1}_{105}$-*b*-$\mathbf{2}_n$) copolymers irradiated at 365 nm. (c) CPL spectra of poly($\mathbf{1}_{105}$-*b*-$\mathbf{2}_n$) irradiated at 380 nm. The spectra were recorded in THF at 25 °C with c = 0.2 mg mL^{-1}.

a maximum when DP = 73. When DP > 73, the $|g_{lum}|$ of the block copolymers decreased. For instance, $|g_{lum}|$ at 480 nm was 5.2 × 10^{-3} for *R*-poly($\mathbf{1}_{105}$-*b*-$\mathbf{2}_{19}$), 6.1 × 10^{-3} for *R*-poly($\mathbf{1}_{105}$-*b*-$\mathbf{2}_{36}$), 8.4 × 10^{-3} for *R*-poly($\mathbf{1}_{105}$-*b*-$\mathbf{2}_{54}$), and 8.9 × 10^{-3} for *R*-poly($\mathbf{1}_{105}$-*b*-$\mathbf{2}_{73}$) (Fig. S14 and S15, ESI†). Furthermore, $|g_{lum}|$ decreased to 8.1 × 10^{-3} for *R*-poly($\mathbf{1}_{105}$-*b*-$\mathbf{2}_{98}$), and 5.9 × 10^{-3} for *R*-poly($\mathbf{1}_{105}$-*b*-$\mathbf{2}_{115}$). This study confirmed that the helical poly-$\mathbf{1}_m$ block induced chiral self-assembly of the π-conjugated block copolymers and formed one-handed helical nanofibers with clear CPL.

Conclusions

In summary, we developed a facile method for precisely synthesising π-conjugated PAM-*b*-PPE block copolymers through living polymerization of two monomers in one pot using a single chiral Pd(II)-catalyst. Although the structure and polymerization mechanism of the two monomers were different, the one-pot block copolymerization proceeded *via* a living chain-growth reaction, affording the desired block copolymers with predictable M_n and low M_w/M_n. The polymerization of achiral monomer **1** using the chiral Pd(II)-catalysts was asymmetric, resulting in polymers that formed preferred one-handed helices. Moreover, the Pd(II)-mediated coordination copolymerization of achiral monomer **2** induced chiral self-assembly of the block copolymers. Well-defined spherical micelles and one-handed supramolecular helical nanofibers with high solid contents were obtained. The assemblies showed high optical activity and clear CPL. We believe this study provides a convenient strategy for the precise synthesis of hybrid block copolymers and a facile method for the construction of optically active supramolecular architectures.

Data availability

The detailed experimental process and additional data associated with this work are available in the ESI.†

Author contributions

Z.-Q. W., L. Z., and N. L. designed and directed the project, R.-T. G., S.-Y. L., and B.-H. L. performed the experiments and analyzed the data. Z.-Q. W., N. L., and Z. C. wrote the manuscript with input from all other authors.

Conflicts of interest

There are no conflicts to declare.

Acknowledgements

This work was supported by the Natural Science Foundation of China (NSFC, No. 92256201, 52273006, 52273204, 22071041, 21971052, and 21871073) and the Fundamental Research Funds for the Central University of China.

Notes and references

1 D. A. Guarracino, J. A. Riordan, G. M. Barreto, A. L. Oldfield, C. M. Kouba and D. Agrinsoni, Macrocyclic Control in Helix Mimetics, *Chem. Rev.*, 2019, **119**, 9915–9949.
2 T. Nakano and Y. Okamoto, Synthetic Helical Polymers: Conformation and Function, *Chem. Rev.*, 2001, **101**, 4013–4038.
3 J.-L. Mergny and D. Sen, DNA Quadruple Helices in Nanotechnology, *Chem. Rev.*, 2019, **119**, 6290–6325.
4 C. J. Whitfield, M. Z. Zhang, P. Winterwerber, Y. Z. Wu, D. Y. W. Ng and T. Weil, Functional DNA–Polymer Conjugates, *Chem. Rev.*, 2021, **121**, 11030–11084.
5 Y.-Y. Zhang, F. Li, M. Li, X.-H. Mao, X.-X. Jing, X.-G. Liu, Q. Li, J. Li, L.-H. Wang, C.-H. Fan and X.-L. Zuo, Encoding Carbon Nanotubes with Tubular Nucleic Acids for Information Storage, *J. Am. Chem. Soc.*, 2019, **141**, 17861–17866.
6 M. Altay, Y. Altay and S. Otto, Parasitic Behavior of Self-Replicating Molecules, *Angew. Chem., Int. Ed.*, 2018, **57**, 10564–10568.
7 M. Rosbash, Circadian Rhythms and the Transcriptional Feedback Loop (Nobel Lecture), *Angew. Chem., Int. Ed.*, 2021, **60**, 8650–8666.
8 E. Yashima, N. Ousaka, D. Taura, K. Shimomura, T. Ikai and K. Maeda, Supramolecular Helical Systems: Helical Assemblies of Small Molecules, Foldamers, and Polymers with Chiral Amplification and Their Functions, *Chem. Rev.*, 2016, **116**, 13752–13990.
9 W. Zhang, W.-S. Jin, T. Fukushima, T. Mori and T. Aida, Helix Sense-Selective Supramolecular Polymerization Seeded by a One-Handed Helical Polymeric Assembly, *J. Am. Chem. Soc.*, 2015, **137**, 13792–13795.
10 C. Lara, N. P. Reynolds, J. T. Berryman, A.-Q. Xu, A.-F. Zhang and R. Mezzenga, ILQINS Hexapeptide, Identified in Lysozyme Left-Handed Helical Ribbons and Nanotubes, Forms Right-Handed Helical Ribbons and Crystals, *J. Am. Chem. Soc.*, 2014, **136**, 4732–4739.
11 H.-Y. Zhang, S. Li, A.-H. Qu, C.-L. Hao, M.-Z. Sun, L.-G. Xu, C.-L. Xu and H. Kuang, Engineering of chiral

nanomaterials for biomimetic catalysis, *Chem. Sci.*, 2020, **11**, 12937–12954.
12 W. Fan, T. Matsuno, Y. Han, X.-H. Wang, Q.-F. Zhou, H. Isobe and J.-S. Wu, Synthesis and Chiral Resolution of Twisted Carbon Nanobelts, *J. Am. Chem. Soc.*, 2021, **143**, 15924–15929.
13 Y. Cakmak, S. Erbas-Cakmak and D. A. Leigh, Asymmetric Catalysis with a Mechanically Point-Chiral Rotaxane, *J. Am. Chem. Soc.*, 2016, **138**, 1749–1751.
14 T. Mori, Chiroptical Properties of Symmetric Double, Triple, and Multiple Helicenes, *Chem. Rev.*, 2021, **121**, 2373–2412.
15 H.-J. Huang, Y.-B. Yuan and J.-P. Deng, Helix-Sense-Selective Precipitation Polymerization of Achiral Monomer for Preparing Optically Active Helical Polymer Particles, *Macromolecules*, 2015, **48**, 3406–3413.
16 A. Satrijo, S. C. J. Meskers and T. M. Swager, Probing a Conjugated Polymer's Transfer of Organization-Dependent Properties from Solutions to Films, *J. Am. Chem. Soc.*, 2006, **128**, 9030–9031.
17 T. Ikai, M. Okubo and Y. Wada, Helical Assemblies of One-Dimensional Supramolecular Polymers Composed of Helical Macromolecules: Generation of Circularly Polarized Light Using an Infinitesimal Chiral Source, *J. Am. Chem. Soc.*, 2020, **142**, 3254–3261.
18 R. Ursin and R. Hughes, Sharing quantum secrets, *Nature*, 2013, **501**, 37–38.
19 Y.-T. Sang, Q.-R. Zhu, X.-Q. Zhou, Y.-Q. Jiang, L. Zhang and M.-H. Liu, Ultrasound-Directed Symmetry Breaking and Spin Filtering of Supramolecular Assemblies from only Achiral Building Blocks, *Angew. Chem., Int. Ed.*, 2023, **62**, e202215867.
20 B. Zhao, X.-B. Gao, K. Pan and J.-P. Deng, Chiral Helical Polymer/Perovskite Hybrid Nanofibers with Intense Circularly Polarized Luminescence, *ACS Nano*, 2006, **15**, 7463–7471.
21 L. A. Warning, A. R. Miandashti, L. A. McCarthy, Q.-F. Zhang, C. F. Landes and S. Link, Nanophotonic Approaches for Chirality Sensing, *ACS Nano*, 2021, **15**, 15538–15566.
22 C. Du, Z.-J. Li, X.-F. Zhu, G.-H. Ouyang and M.-H. Liu, Hierarchically self-assembled homochiral helical microtoroids, *Nat. Nanotechnol.*, 2022, **17**, 1294–1302.
23 S.-L. Cai, Y.-H. Huang, S.-Y. Xie, S. Wang, Y. Guan, X.-H. Wan and J. Zhang, 2D Hexagonal Assemblies of Amphiphilic Double-Helical Poly(phenylacetylene) Homopolymers with Enhanced Circularly Polarized Luminescence and Chiral Self-Sorting, *Angew. Chem., Int. Ed.*, 2022, **61**, e202214293.
24 X.-C. Ye, B.-W. Li, Z.-X. Wang, J. Li, J. Zhang and X.-H. Wan, Tuning organic crystal chirality by the molar masses of tailored polymeric additives, *Nat. Commun.*, 2021, **12**, 6841.
25 T.-J. Yue, W.-M. Ren, L. Chen, G.-G. Gu, Y. Liu and X.-B. Lu, Synthesis of Chiral Sulfur-Containing Polymers: Asymmetric Copolymerization of meso-Epoxides and Carbonyl Sulfide, *Angew. Chem., Int. Ed.*, 2018, **57**, 12670–12674.
26 T. Sakamoto, Y. Fukuda, S. Sato and T. Nakano, Photoinduced Racemization of an Optically Active Helical Polymer Formed by the Asymmetric Polymerization of 2,7-Bis(4-tert-butylphenyl)fluoren-9-yl Acrylate, *Angew. Chem., Int. Ed.*, 2009, **48**, 9308–9311.
27 J. Luo and K. J. Shea, Polyhomologation. A Living C1 Polymerization, *Acc. Chem. Res.*, 2010, **43**, 1420–1433.
28 C. R. Caboon and C. W. Bielawski, Metal-promoted C1 polymerization, *Coord. Chem. Rev.*, 2018, **374**, 261–278.
29 A. I. O. Suarez, M. P. del Río, K. Remerie, J. N. H. Reek and B. de Bruin, Rh-Mediated C1-Polymerization: Copolymers from Diazoesters and Sulfoxonium Ylides, *ACS Catal.*, 2012, **2**, 2046–2059.
30 E. Ihara, V. G. Young and R. F. Jordan, Cationic Aluminum Alkyl Complexes Incorporating Aminotroponiminate Ligands, *J. Am. Chem. Soc.*, 1998, **120**, 8277–8278.
31 Y. Ito, E. Ihara, M. Murakami and M. Shiro, New living polymerization of 1,2-diisocyanoarenes via (quinoxalinyl) palladium complexes. Synthesis of poly(2,3-quinoxaline), *J. Am. Chem. Soc.*, 1990, **112**, 6446–6447.
32 J.-H. Chu, X.-H. Xu, S.-M. Kang, N. Liu and Z.-Q. Wu, Fast Living Polymerization and Helix-Sense-Selective Polymerization of Diazoacetates Using Air-Stable Palladium(II) Catalysts, *J. Am. Chem. Soc.*, 2018, **140**, 17773–17781.
33 X.-Q. Yao, Y.-S. Wang and J.-B. Wang, Cp(π-Allyl)Pd-Initiated Polymerization of Diazoacetates: Reaction Development, Kinetic Study, and Chain Transfer with Alcohols, *Macromolecules*, 2021, **54**, 10914–10922.
34 S. Kang, S. J. Lu and C. W. Bielawski, C1 Polymerization of Fluorinated Aryl Diazomethanes, *ACS Macro Lett.*, 2022, **11**, 7–14.
35 L. Zhou, R.-T. Gao, X.-J. Zhang, K. He, L. Xu, N. Liu and Z.-Q. Wu, A Versatile Method for the End-Functionalization of Polycarbenes, *Macromol. Rapid Commun.*, 2022, **43**, 2100630.
36 X.-H. Xu, W.-B. Liu, X. Song, L. Zhou, N. Liu, Y.-Y. Zhu and Z.-Q. Wu, Chain-end functionalization of living helical polyisocyanides through a Pd(II)-mediated Sonogashira coupling reaction, *Polym. Chem.*, 2021, **12**, 4838–4845.
37 S. Kang, R. J. Ono and C. W. Bielawski, Controlled Catalyst Transfer Polycondensation and Surface-Initiated Polymerization of a p-Phenyleneethynylene-Based Monomer, *J. Am. Chem. Soc.*, 2013, **135**, 4984–4987.
38 L. Zhou, X.-H. Xu, Z.-Q. Jiang, L. Xu, B.-F. Chu, N. Liu and Z.-Q. Wu, Selective Synthesis of Single-Handed Helical Polymers from Achiral Monomer and a Mechanism Study on Helix-Sense-Selective Polymerization, *Angew. Chem., Int. Ed.*, 2021, **60**, 806–812.
39 X.-X. Cheng, T.-F. Miao, Y.-F. Ma, X.-Y. Zhu, W. Zhang and X.-L. Zhu, Controlling the Multiple Chiroptical Inversion in Biphasic Liquid-Crystalline Polymers, *Angew. Chem., Int. Ed.*, 2021, **60**, 24430–24436.
40 S.-L. Cai, J.-X. Chen, S. Wang, J. Zhang and X.-H. Wan, Allostery-Mimicking Self-assembly of Helical Poly(phenylacetylene) Block Copolymers and the Chirality Transfer, *Angew. Chem., Int. Ed.*, 2021, **60**, 9686–9692.
41 L.-B. Gao, X.-Q. Dou, C. Xing, F.-L. Gao, Z.-C. Jiang, K.-K. Yang, C.-L. Zhao and C.-L. Feng, Realizing Abundant Chirality Inversion of Supramolecular Nano helices by

Multiply Manipulating the Binding Sitesin Molecular Blocks, *Angew. Chem., Int. Ed.*, 2023, **62**, e202303812.

42 X.-Y. Zhang, Z.-R. Xu, Y. Zhang, Y.-W. Quan and Y.-X. Cheng, Controllable Circularly Polarized Electroluminescence Performance Improved by the Dihedral Angle of Chiral-Bridged Binaphthyl-Type Dopant Inducers, *ACS Appl. Mater. Interfaces*, 2021, **13**, 55420–55427.

43 X.-N. Han, Y. Han and C.-F. Chen, Supramolecular tessellations by the exo-wall interactions of pagoda[4] arene, *Nat. Commun.*, 2021, **12**, 6378.

44 M. Douverne, Y. Ning, A. Tatani, F. C. Meldrum and S. P. Armes, How Many Phosphoric Acid Units Are Required to Ensure Uniform Occlusion of Sterically Stabilized Nanoparticles within Calcite?, *Angew. Chem., Int. Ed.*, 2019, **58**, 8692–8697.

45 F. H. Sobotta, M. T. Kuchenbrod, F. V. Gruschwitz, G. Festag, P. Bellstedt, S. Hoeppener and J. C. Brendel, Tuneable Time Delay in the Burst Release from Oxidation-Sensitive Polymersomes Made by PISA, *Angew. Chem., Int. Ed.*, 2021, **60**, 24716–24723.

46 L. Wan, R. Ruiz, H. Gao and T. R. Albrecht, Self-Registered Self-Assembly of Block Copolymers, *ACS Nano*, 2017, **11**, 7666–7673.

47 D. H. Kim, B.-L. Lee, H. Moon, H. M. Kang, E. J. Jeong, J. Park, K.-M. Han, S. Lee, B. W. Yoo, B. W. Koo, J. Y. Kim, W. H. Lee, K. Cho, H. A. Becerril and Z. Bao, Liquid-Crystalline Semiconducting Copolymers with Intramolecular Donor−Acceptor Building Blocks for High-Stability Polymer Transistors, *J. Am. Chem. Soc.*, 2009, **131**, 6124–6132.

48 Z. Geng, B.-J. Xiong, L.-Q. Wang, K. Wang, M. Ren, L.-B. Zhang, J.-T. Zhu and Z.-Z. Yang, Moebius strips of chiral block copolymers, *Nat. Commun.*, 2019, **10**, 4090.

49 Q.-C. Zhang, R.-M. Zeng, Y.-X. Zhang, Y. Chen, L. Zhang and J.-B. Tan, Two Polymersome Evolution Pathways in One Polymerization-Induced Self-Assembly (PISA) System, *Macromolecules*, 2020, **53**, 8982–8991.

50 Y. Zhang, M.-J. Cao, G. Han, T.-Y. Guo, T.-Y. Ying and W.-Q. Zhang, Topology Affecting Block Copolymer Nanoassemblies: Linear Block Copolymers versus Star Block Copolymers under PISA Conditions, *Macromolecules*, 2018, **51**, 5440–5449.

51 F. D'Agosto, J. Rieger and M. Lansalot, RAFT-Mediated Polymerization-Induced Self-Assembly, *Angew. Chem., Int. Ed.*, 2020, **59**, 8368–8392.

52 B. Fan, J. Wan, J.-L. Zhai, X.-Y. Chen and S. H. Thang, Triggered Degradable Colloidal Particles with Ordered Inverse Bicontinuous Cubic and Hexagonal Mesophases, *ACS Nano*, 2021, **15**, 4688–4698.

53 S. Kushida, E. Smarsly, N. M. Bojanowski, I. Wacker, R. R. Schröder, O. Oki, Y. Yamamoto, C. Melzer and U. H. F. Bunz, Dipole-Switchable Poly(para-phenyleneethynylene)s: Ferroelectric Conjugated Polymers, *Angew. Chem., Int. Ed.*, 2018, **57**, 17019–17022.

54 L. Arnt and G. N. Tew, New Poly(phenyleneethynylene)s with Cationic, Facially Amphiphilic Structures, *J. Am. Chem. Soc.*, 2002, **124**, 7664–7665.

55 J. Lim and T. M. Swager, Fluorous Biphase Synthesis of a Poly(p-phenyleneethynylene) and its Fluorescent Aqueous Fluorous-Phase Emulsion, *Angew. Chem., Int. Ed.*, 2010, **49**, 7486–7488.